water

MDPI

Article

Cryptophyte and Photosynthetic Picoeukaryote Abundances in the Bransfield Strait during Austral Summer

Vladimir Mukhanov [1,*], Evgeny Sakhon [1], Alexander Polukhin [2], Vladimir Artemiev [2], Eugene Morozov [2] and An-Yi Tsai [3,4]

[1] A. O. Kovalevsky Institute of Biology of the Southern Seas, Russian Academy of Sciences, 299011 Sevastopol, Russia; sachon@mail.ru
[2] Shirshov Institute of Oceanology, Russian Academy of Sciences, 117997 Moscow, Russia; aleanapol@gmail.com (A.P.); artemiev195@yandex.ru (V.A.); egmorozov@mail.ru (E.M.)
[3] Institute of Marine Environment and Ecology, National Taiwan Ocean University, Keelung 202-24, Taiwan; anyitsai@mail.ntou.edu.tw
[4] Center of Excellence for the Oceans, National Taiwan Ocean University, Keelung 202-24, Taiwan
* Correspondence: v.s.mukhanov@ibss-ras.ru; Tel.: +7-978-7239140

Abstract: A remarkable shift in the species composition and size distribution of the phytoplankton community have been observed in coastal waters along the Antarctic Peninsula over the last three decades. Smaller photoautotrophs such as cryptophytes are becoming more abundant and important for the regional ecosystems. In this study, flow cytometry was used to quantify the smallest phytoplankton in the central Bransfield Strait and explore their distribution across the strait in relation to physical and chemical properties of the two major water masses: the warmer and less saline Transitional Zonal Water with Bellingshausen Sea influence (TBW), and the cold and salty Transitional Zonal Water with Weddell Sea influence (TWW). Pico- and nano-phytoplankton clusters were distinguished and enumerated in the cytograms: photosynthetic picoeukaryotes, cryptophytes (about 9 μm in size), and smaller (3 μm) nanophytoplankton. It was shown that nanophytoplankton developed higher abundances and biomasses in the warmer and less saline TBW. This biotope was characterized by a more diverse community with a pronounced dominance of Cryptophyta in terms of biomass. The results support the hypothesis that increasing melt-water input can potentially support spatial and temporal extent of cryptophytes. The replacement of large diatoms with small cryptophytes leads to a significant shift in trophic processes in favor of the consumers such as salps, which able to graze on smaller prey.

Keywords: cryptophytes; nanophytoplankton; picophytoplankton; photosynthetic picoeukaryotes; phytoplankton bloom; Bransfield Strait; Antarctic Peninsula; flow cytometry

Citation: Mukhanov, V.; Sakhon, E.; Polukhin, A.; Artemiev, V.; Morozov, E.; Tsai, A.-Y. Cryptophyte and Photosynthetic Picoeukaryote Abundances in the Bransfield Strait during Austral Summer. *Water* **2022**, *14*, 185. https://doi.org/10.3390/w14020185

Academic Editors: Michele Mistri, Maria Moustaka-Gouni and Jun Yang

Received: 16 November 2021
Accepted: 29 December 2021
Published: 10 January 2022

1. Introduction

Diatoms, haptophytes (predominantly *Phaeocystis antarctica*), and cryptophytes represent the major taxonomic groups of phytoplankton in the Southern Ocean [1–5]. Summer phytoplankton blooms in coastal waters of the Antarctic Peninsula are usually associated with a shallow upper mixed layer (UML) that keeps phytoplankton under favorable light conditions and better supply of dissolved iron (e.g., [6]). As a rule, diatoms and/or *P. antarctica* make the largest contribution to the blooms, but the role of cryptophytes has been reported to substantially increase, especially in water areas of melting glaciers [7–9]. The mechanisms behind Cryptophyta bloom formation are still poorly understood. Lower water temperatures in the surface layer, narrowing of the UML and a decrease in water salinity appear to favor the development of the phenomenon [9,10].

Publicly available data provide evidence of the transformation of the Antarctic phytoplankton community as a probable consequence of global warming [10]. The transformation covers not only taxonomic composition but also the size structure of the community. The

replacement of large diatoms with small cryptophytes leads to a significant shift in trophic processes in favor of the consumers able to graze on smaller prey. Since Antarctic krill is not one of them [11], such a trend gives rise to a well-founded concern. A decrease in the food supply of krill and a substitution of the latter by other zooplankton (such as salps) imply a reduction in the carbon pool available for higher trophic levels by almost 70% [12].

It was shown in a number of experimental studies that Antarctic krill feed on small prey (about 10 μm in size) with low efficiency [13,14], while the optimal size of its food objects is about 50 μm due to the features of the filtration apparatus of euphausiids [13]. This well explains why krill exhibit positive selectivity for diatoms and avoid cryptophytes when feeding on complex prey mixtures [11].

On the contrary, salps, a food competitor of Antarctic krill, are satisfied with a wide range of taxonomic and size composition of phytoplankton prey thus demonstrating much lower feeding selectivity [11]. Against the background of their ongoing expansion to higher latitudes [12,15], their potential ability to utilize the biomass of cryptophytes during phytoplankton bloom periods poses additional threats to Antarctic krill populations, and hence, also for higher consumers including penguins, seals, and whales which feed on krill [16]. Thus, an increasing role of Cryptophyta in the Antarctic waters implies restrictions in food supply for krill and strengthening of its competitor's position.

The phenomenon of increasing cryptophyte abundances in the Antarctic waters have been initially explained by advection [7], sedimentation of large diatoms [17], grazing [2], and tolerance of cryptophytes to lower salinity waters [8]. Recently, Mendes et al. [18] studied the prevalence of cryptophytes in the coastal waters of the western Antarctic Peninsula and hypothesized that the phenomenon can be due to their pigment protection capability and, as a result, an ability to successfully grow under high irradiance exposure in strongly stratified shallow mixing surface layers. In this context, our major objective was to characterize the nanophytoplankton assemblage (2 to 20 μm in size) by flow cytometry (FCM), identify the Cryptophyta component, and analyze their distribution in the water masses of the Bransfield Strait, differing significantly from each other and the rest of the western Antarctic Peninsula shelf by their physical and chemical properties. Special attention was paid to nanophytoplankton of the transitional water mass with Bellingshausen Sea influence, which is warmer and fresher due to melting ice. We tested the hypothesis that an increase in melt-water input can potentially promote the spatial and temporal extent of cryptophytes.

Additionally, we used FCM to enumerate the smallest known component of the phytoplankton community, picophytoplankton (0.2 to 2.0 μm size fraction), which are recognized as an important player in the Southern Ocean ecosystem. In this part of the work, we focused on revealing spatial patterns of picophytoplankton abundance in relation to the water masses and frontal zones in the Bransfield Strait as the frontal features are among the factors other than temperature that control the abundance and distribution of phytoplankton.

2. Materials and Methods

2.1. Sampling Sites and Methods

The oceanographic and microbiological data were collected on 21 January 2020 over a transect across the central Bransfield Strait (BS) (7 stations, Figure 1) during 79th cruise of the R/V "Akademik Mstislav Keldysh". The length of the transect from Greenwich Island (South Shetland Islands) to the shelf of the Antarctic Peninsula was 93 km. Water samples were taken at 5 to 7 depths from the surface to 190 m, depending on the hydrological structure and chlorophyll *a* (Chl-*a*) fluorescence distribution.

The water area sufficiently differs from the rest of the western Antarctic Peninsula shelf by the inflow of cold and saline Weddell Sea shelf water [18,19]. According to Tokarczyk's classification [20], the water masses in the BS are the Transitional Zonal Water with Bellingshausen Sea influence (TBW; water temperature $T > 1$ °C, salinity $S < 34.1$ psu), and the Transitional Zonal Water with Weddell Sea influence (TWW; $T < 1$ °C, $S > 34.1$ psu).

Figure 2 represents water temperature profiles at the stations (6587–6595) along the transect in the BS and the front between TBW and TWW. These waters are separated from each other by a shallow hydrographic front which has a clear surface thermal signature. The 1 °C isotherm serves as a good boundary between TBW and TWW in summer. TBW occupies only a 50-m thick upper layer along the South Shetland Islands whereas the rest of the Bransfield basin is occupied by TWW [21].

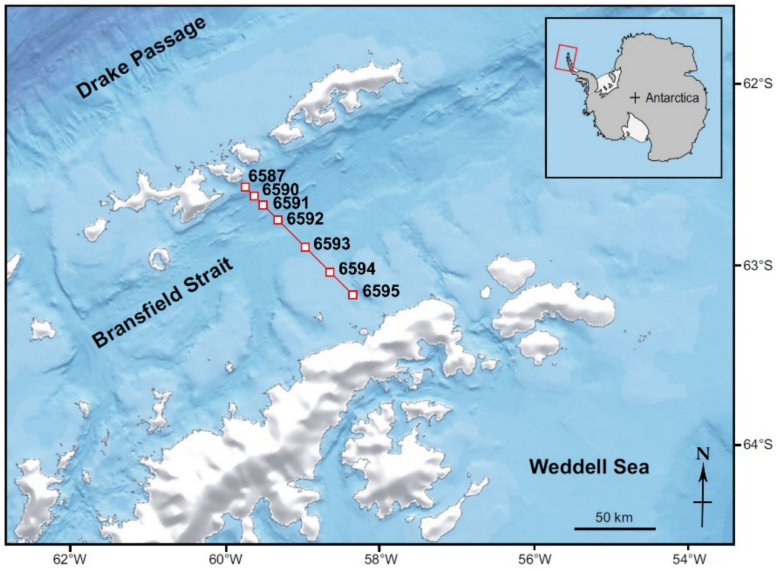

Figure 1. Location of oceanographic stations in the Bransfield Strait (79th cruise of R/V "Akademik Mstislav Keldysh", January 2020) where water samples were collected at 5 to 7 depths in austral mid-summer.

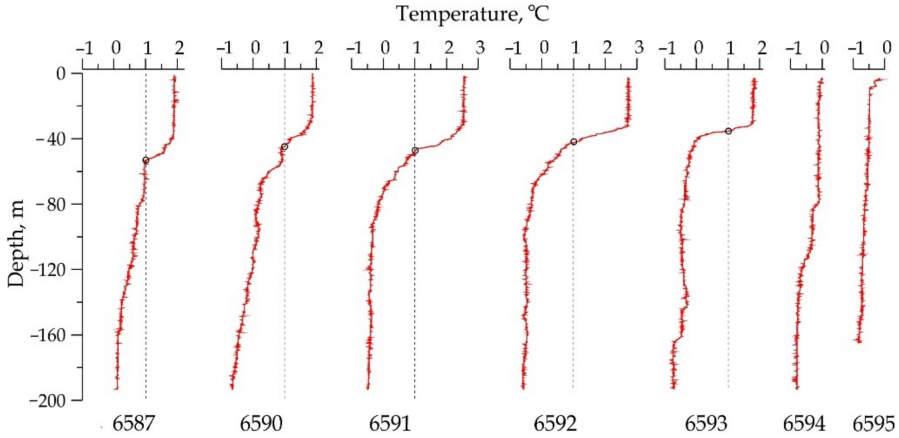

Figure 2. Water temperature profiles at the stations (6587–6595) along the transect in the Bransfield Strait. The depths of 1 °C isotherm (marked with empty circles) corresponded to the front between TBW and TWW.

2.2. Physical and Chemical Oceanographic Data

Temperature, conductivity, and pressure data were collected using a SBE911 CTD attached to a Carrousel system with 24 5-L Niskin bottles for water sampling. Current velocity profiles were measured by a Workhorse Sentinel ADCP. Profile measurements of Chl-*a* concentration and photosynthetically active radiation (PAR) were conducted using a PUM-200 transparency meter equipped with a Minitracka-II fluorimeter (Chelsey Instruments Ltd., Surrey, UK), and a LI-COR radiometer equipped with two LI-192 sensors.

Dissolved oxygen and nutrients were immediately measured onboard in all of the samples using a modified Winkler method [22] and standard colorimetric methods [23–26].

2.3. Flow Cytometry

Water samples were fixed (2% formaldehyde fin. conc.) and frozen on board in liquid nitrogen for their storage and transportation to a stationary laboratory before flow-cytometric analysis. No fractionation was employed with the exception of screening the sample through the 70-µm nylon mesh to avoid clogging the fluidic system of the instrument by larger objects (detritus, microalgae, zooplankton, etc.). Taxonomic composition and abundance of the micro-phytoplankton were not studied.

Cytometric gating and sizing of pico- and nanophytoplankton were performed using a Cytomics^{TM} FC 500 flow cytometry system (Beckman Coulter Inc., Brea, CA, USA) and Flowing Software v. 2.5.0 (Perttu Terho, Turku Centre for Biotechnology, University of Turku, Finland, https://bioscience.fi/services/cell-imaging/flowing-software/, released 4 November 2013). The standard forward light scatter (FSC), orange fluorescence (FL2, 575 nm), and red fluorescence (FL4, 675 nm) channels were used for the acquisition and analysis.

Two nanophytoplankton clusters were distinguished and enumerated, namely cryptophytes (CP) and other nanophytoplankton (NP). Cryptophytes contain a distinctive set of pigments, the orange fluorescing phycobilins (although there are also colorless members, [27]. These cryptomonads were identified by their bright orange fluorescence while NP did not produce it (Figure 3). The light microscopy observation of cryptomonad cells confirmed the flow cytometry data. The FL4 and FL2 values measured in individual cells served a measure of their intracellular Chl-*a* and phycoerythrin (PE) contents, respectively [28]. Picophytoplankton were dominated by photosynthetic picoeukaryotes (PPE) while abundances of picocyanobacteria were extremely low or undetectable. For this reason, we identified and enumerated PPE only, according to Marie et al. [29] (Figure 3).

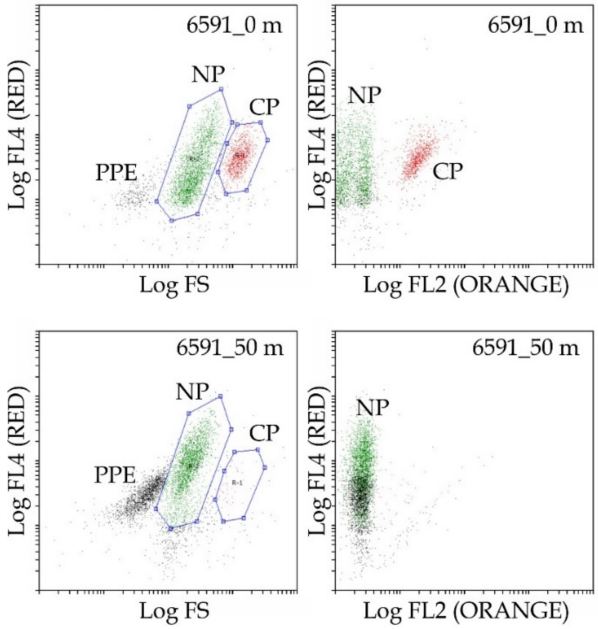

Figure 3. Gating cryptophytes (CP), other nanophytoplankton (NP) and photosynthetic picoeukaryotes (PPE) in the space of forward light scattering (FS is cell size), red autofluorescence (FL4 is Chl-*a*) and orange autofluorescence (FL2 is phycoerythrin) in two samples (station 6591 at 0 and 50 m).

Cell size measurements were calibrated in terms of equivalent spherical diameter (ESD, µm), using a set of standard polystyrene beads (Polysciences, Inc., Warrington, PA, USA) in the size range between 0.5 and 10 µm; calibration curves were obtained for each flow cytometry protocol by plotting the ESD as a function of the FSC signal (coefficient of determination $r^2 > 0.8$ in all cases). Mean ESD and cell volume were calculated for every cell population from the calibration curves [30]. To allow for a better comparison with earlier published data, nanophytoplankton abundances and biovolumes were converted to

cellular carbon (C). Carbon conversion factors were shown to vary depending on taxonomy, cell size, and growth-regulating factors such as light and nutrient availability [31]. In this study, carbon content of pico- and nanophytoplankton was estimated from the mean ESD using the conversion factors of 237 fg C μm^{-3} [32] and 196.5 fg C μm^{-3} [33], respectively.

2.4. Statistics

Multivariate statistical analysis (cluster analysis and non-metric multi-dimensional scaling, nMDS) of microbiological and hydrological-hydrochemical data collected in the upper 190-m layer was carried out using the PAST3 software [34]. Mapping the spatial distribution of the variables and graph plotting were performed using Surfer v. 10 and Grapher v. 8 software (Golden Software, Inc., Golden, CO, USA), respectively.

In total, 24 biological, hydrological and hydrochemical variables were measured in the study site and investigated by the methods of multivariate statistical analysis (Table 1). The 12 microbiological variables included in this list characterized both the structure (*CPN*, *CPN%*, *CPB%*, *NPN*, *NPB*, *CP-ESD*, *NP-ESD*, *PPEN*, *PPEB*, *PPE-ESD*) and some functional characteristics of the communities namely, intracellular content of photosynthetic pigments in the photoautotrophic cells (*CP-CHL*, *CP-PE*, *NP-CHL*, *PPE-CHL*).

Table 1. Symbols of variables used in this study with their definitions, units, and descriptive statistics (n = 39). R. u. is relative units, CP is cryptophyte, NP is nanoplankton, PPE is photosynthetic picoeukaryotes, ESD is equivalent spherical diameter, SD is standard deviation.

Symbol	Definition, Units	Min	Max	Mean ± SD
T	Water temperature, °C	−0.79	2.77	0.59 ± 1.19
S	Water salinity, psu	34.1	34.4	34.3 ± 0.1
PO4	Phosphates, μM	1.56	4.37	3.09 ± 0.58
Si	Silicates, μM	67.9	112.3	81.3 ± 10.1
NO3	Nitrates, μM	22.6	35.4	29.4 ± 3.7
NO2	Nitrites, μM	0.11	0.23	0.17 ± 0.04
NH4	Ammonium, μM	1.32	3.81	2.13 ± 0.58
DO	Dissolved oxygen, mL L^{-1}	6.44	7.98	7.44 ± 0.36
FLUOR	Chl-*a* fluorescence, r. u.	0.10	0.49	0.24 ± 0.12
CPN	Cryptophyte abundance, 10^6 cells L^{-1}	0.00	1.55	0.35 ± 0.46
CP-ESD	Mean CP ESD, μm	6.70	11.59	9.42 ± 1.77
CPB	CP biomass, μg C L^{-1}	0	179	33 ± 45
CP-CHL	Intracellular Chl-*a* content in CP, r. u. cell $^{-1}$	0	163	69 ± 39
CP-PE	Intracellular phycoerythrin content in CP, r. u. cell $^{-1}$	0	206	31 ± 39
NPN	NP abundance, 10^6 cells L^{-1}	0.19	3.95	1.71 ± 1.07
NP-ESD	Mean NP ESD, μm	2.14	3.67	2.88 ± 0.38
NPB	NP biomass, μg C L^{-1}	0.4	15.7	4.3 ± 3.2
NP-CHL	Intracellular Chl-*a* content in NP, r. u. cell $^{-1}$	8	220	74 ± 52
TNPB	Total NP+CP biomass, μg C L^{-1}	0.4	194.2	37.3 ± 47.7
CPN%	Proportion of CP in the total abundance, %	0	49	14 ± 12
CPB%	Proportion of CP in the total biomass, %	0	96	74 ± 21
PPEN	PPE abundance, 10^6 cells L^{-1}	0.06	4.18	0.87 ± 1.03
PPE-ESD	Mean PPE ESD, μm	1.72	2.09	1.90 ± 0.11
PPEB	PPE biomass, μg C L^{-1}	0.04	3.50	0.72 ± 0.83

3. Results

3.1. Description of Oceanographic Features

Vertical distribution of water temperature and salinity across the BS (Figure 4) corresponded to the typical BS circulation system, with the Southern BS Current carrying waters advected from the Weddell Sea and meeting the relatively warm and less saline waters from the western Antarctic Peninsula through the Gerlache Strait Current at the western end of the BS [35,36]. Together they feed into the eastward flowing Bransfield Current, which is a baroclinic jet directed from the southwest to the northeast and transporting TBW along the southern slope of the Southern Shetland Islands [35–39]. The highest Bransfield Current velocity (0.45 m s^{-1}) was observed at station 6590 in the surface layer. The inflow of cold and saline Weddell Sea Shelf Water was recorded at station 6594 over the entire range of water depths (0 to 200 m) with the maximum velocity of about 0.15 m s^{-1}.

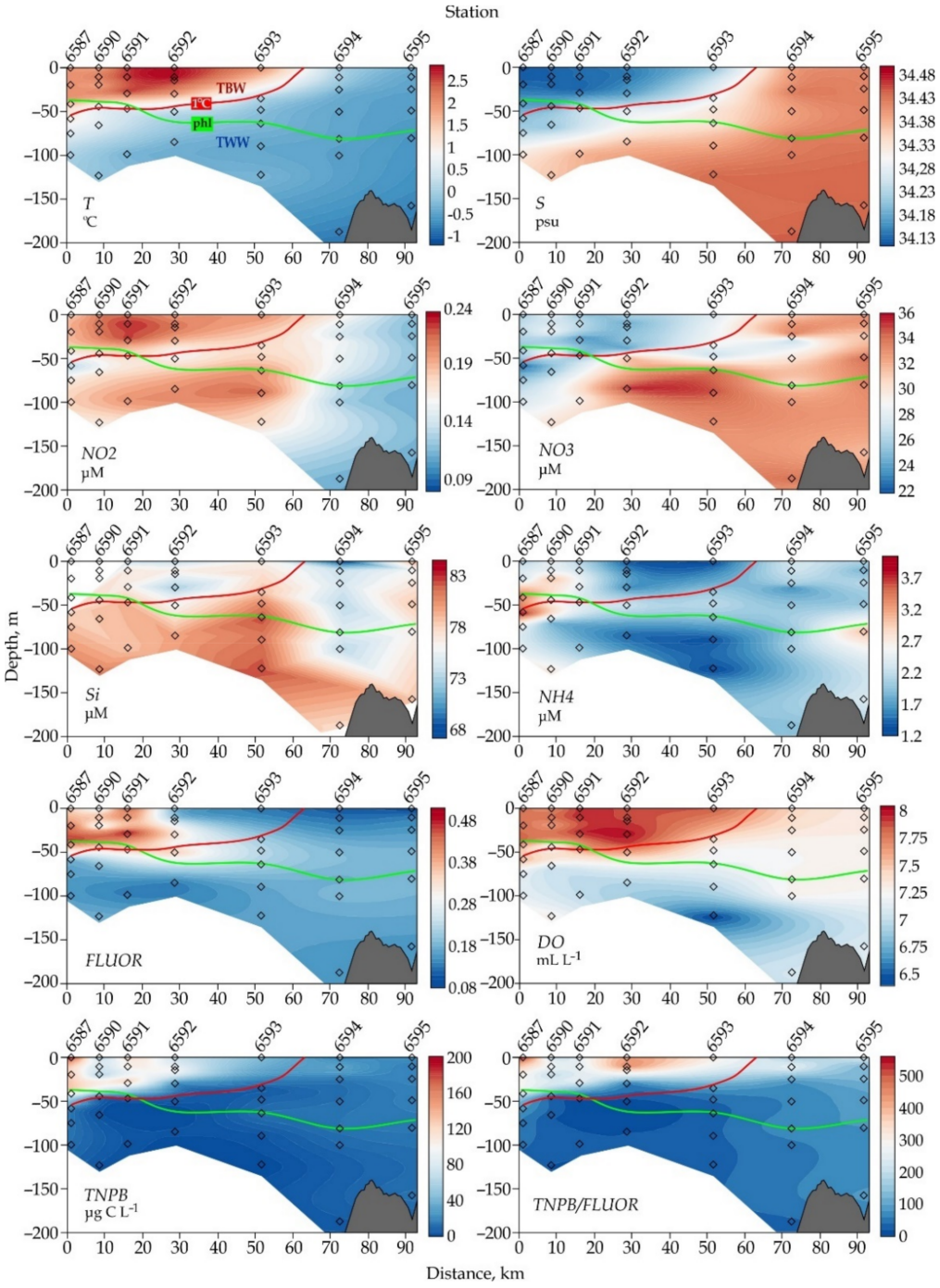

Figure 4. Vertical distribution of water temperature (*T*), salinity (*S*), nutrients (*NO2*, *NO3*, *NH4*, *Si*), dissolved oxygen (*DO*), Chl-*a* fluorescence (*FLUOR*), total nanophytoplankton biomass (*TNPB*), and *TNPB/FLUOR* ratio along the transect in the Bransfield Strait during austral mid-summer, January 2020. Green and red lines represent the bottom of the euphotic layer (phl) and 1 °C isotherm (as a boundary between TBW and TWW; explanations are in the text), respectively. Description of the variables is given in Table 1.

At the surface, warmer and less saline TBW occupied most of the BS (from station 6587 to 6593, Figure 4). Between stations 6593 and 6594, the 2 water masses were separated from each other in the surface layer by the Bransfield Front [37,38]. Being a conventional boundary between the water masses in the BS [20], the 1 °C isotherm did not deepen below

50 m (station 6587) and also corresponded to the maximum temperature gradient (marked in Figure 2 with empty circles).

The offshore waters of the South Shetland Islands are subject to local heating and meltwater inflow [40], which also affects the oxygen distribution in the northern part of the BS. During the study period, near-surface oxygen concentration reached 8.0 mL L^{-1} (Table 1, Figure 4), with oxygen saturation ranging between 100% and 104%. High ammonium nitrogen concentrations (1.0 to 3.8 μM) (Figure 4) were apparently associated with both organic matter oxidation as a result of active phytoplankton bloom and runoff of meltwater from the shores of the South Shetland Islands [19]. Concentrations of nitrite nitrogen (about 0.2 μM) also indicated an active decomposition of organic matter against the background of high primary production in TBW [19] (Figure 4). Nitrate nitrogen concentration varied between 22 and 35 μM, with the highest values observed below 50-m depth in the central part of the transect. In the upper 200-m layer, dissolved silicate concentration was the highest (up to 112 μM) in the northern part of the strait (Figure 4).

The euphotic layer was within the upper 40 m in the northern part of the transect and extended to about 80 m in the TWW water mass at station 6594 (Figure 4). The highest Chl-*a* fluorescence values were measured at the northern stations (6587, 6590, 6591) at the depths between 0 and 50 m within TBW (Figure 4). The maximum of Chl-*a* (1.28 μg L^{-1}) and high *DO* values (up to 8 mL L^{-1}) were observed at station 6591, providing evidence of phytoplankton bloom in the water area [19,41]. At the same time, meltwater conditions of TBW may also affect bio-optical properties of the surface waters in the BS [42].

3.2. Picophytoplankton

Abundance and biomass of PPE averaged 0.87 ± 1.03 × 10^6 cells L^{-1} and 0.72 ± 0.83 μg C L^{-1}, respectively (Table 1). They preferred deeper, colder layer below the <1 °C isotherm, thus, demonstrating their association with TWW (Figure 5). The highest PPE abundance and biomass were observed at 50-m depth at station 6593. In the patch, these values reached 4.18 × 10^6 cells L^{-1} and 3.5 μg C L^{-1}, respectively. In the surface layer, PPE were relatively abundant at the front between TWW and TBW.

3.3. Nanophytoplankton

CP were significantly less abundant (0.35 ± 0.46 × 10^6 cells L^{-1}; ± SD is presented here and further) than NP (1.71 ± 1.07 × 10^6 cells L^{-1}); however, their cells were much larger (about 9.5 μm versus 3 μm in NP). Hence, their average carbon biomass (33 ± 45 μg C L^{-1}) significantly exceeded those of NP (4.3 ± 3.2 μg C L^{-1}) (Table 1). The average cryptophyte ESD measured by flow cytometry (9.4 ± 1.8 μm) slightly exceeded the estimates (8 ± 2 μm) obtained earlier for Antarctic cryptophytes, using light microscopy [43]. Contribution of Cryptophyta to the total nanophytoplankton abundance and biomass reached 49% and 96%, respectively, with the average values of 14 ± 12% and 74 ± 21% (Table 1). The Cryptophyta biomass maximum (about 180 μg C L^{-1}) was observed in TBW in the northern part of the transect (station 6587).

Patches of the highest CP abundance and biomass were observed in the euphotic layer around the jet of the Bransfield Current (station 6590, surface layer) while in TWW (i.e., below the 1 °C isotherm), cryptophytes were scarce or undetectable, especially in the deeper layers (Figure 5). The NP demonstrated similar distribution pattern with the highest abundances at 35–50 m depth at station 6591 (Figure 5). The maximum contribution of CP to the total nanophytoplankton biomass was recorded farther south in TBW (stations 6591 and 6592) at shallow depths (about 10 m) where NP were not abundant (Figure 5).

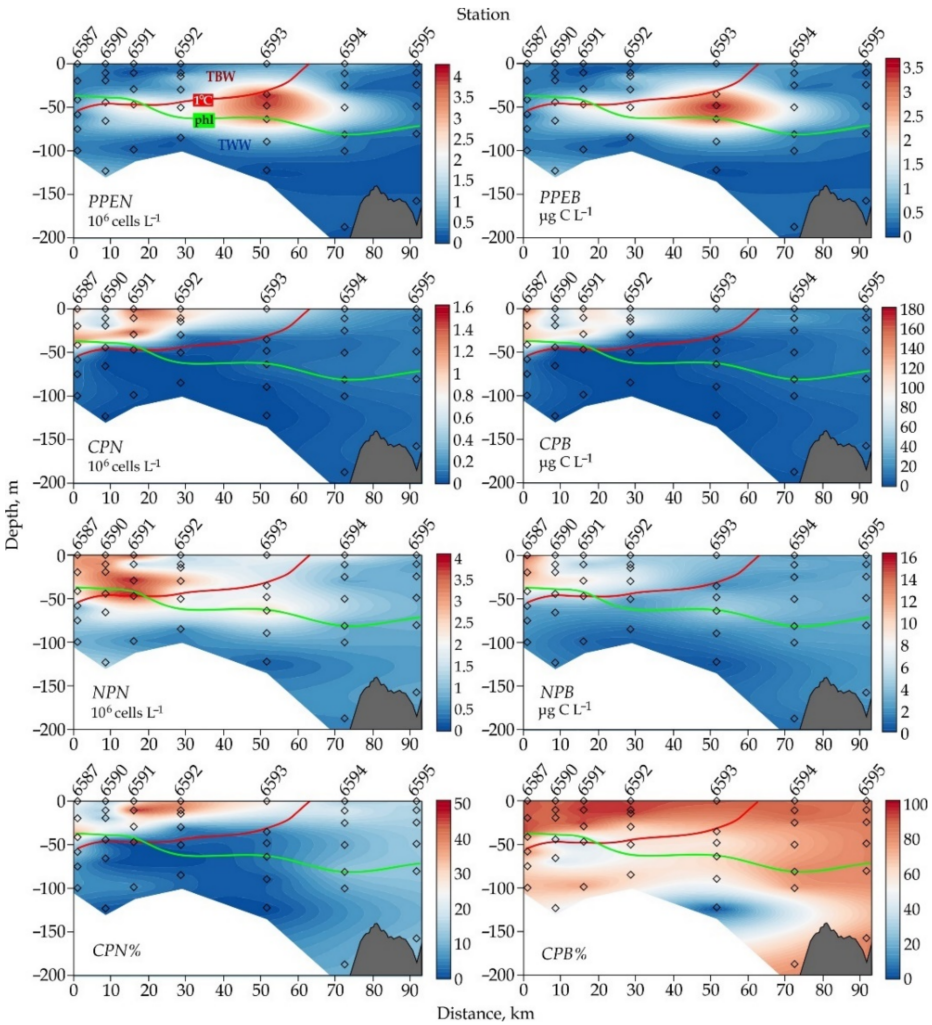

Figure 5. Vertical distribution of photosynthetic picoeukaryote (*PPEN*, *PPEB*), cryptophytes (*CPN*, *CPB*, *CPN%*, *CPB%*), and other nanophytoplankton (*NPN*, *NPB*) along the transect in the Bransfield Strait during austral mid-summer, January 2020. Green and red lines represent the bottom of the euphotic layer (phl) and 1 °C isotherm (as a boundary between TBW and TWW; explanations are in the text), respectively. Description of the variables is in Table 1.

4. Discussion

4.1. Picoeukaryotes

Undetectable levels of prokaryotic picophytoplankton in the study site were not surprising since these microorganisms tend to be scarce or absent in polar region. Their abundance is often inversely related to picoeukaryotes, which are favored by more physically active mixed layers (e.g., [44]). According to the data synthesis by Buitenhuis et al. [45], picoeukaryotes dominate by >75% poleward of 40°. Thus, in the Antarctic waters, picophytoplankton are mostly represented by picoeukaryotes. Moreover, they may occasionally contribute up to 100% of the autotrophic biomass in subsurface waters of the BS [46].

The picoeukaryote concentrations reported in this study were relatively low compared to the data collected earlier in the summer picophytoplankton community [45–47]. In the BS waters, PPE abundance varied from 6 to 14 $\times$ 10^6 cells L^{-1} during summer 2000 [46] that was significantly higher than our estimates. According to Lin et al. [48], the highest PPE summer abundance appeared offshore in the Southwest Atlantic Ocean and changed from 0.2 to 18.2 $\times$ 10^6 cells L^{-1}, with an average of 3.2 $\times$ 10^6 cells L^{-1}. PPE biomass estimates reported in the above study (0.03 to 38.2 µg C L^{-1}) also substantially exceeded

our results, with neither water temperature nor salinity having significant correlation with the picoeukaryote biomass.

Picoeukaryotes demonstrated statistically significant ($p < 0.05$) correlation with water temperature (0,35), salinity (–0.39), phosphates (0.41), and total Chl-*a* (0.45) (Table 2) but this did not provide any explanation of the low PPE abundance and their patchy distribution in the BS waters. Contrary to expectations from the correlation analysis, the PPE 'patch' was situated in the colder and more saline TWW just below the front between the water masses. This may support a suggestion that the nanophytoplankton over-competed the PPE in TBW, forcing them to stay outside the Cryptophyta bloom. Other factors such as frontal dynamics and light penetration also may be important. In particular, despite picophytoplankton ability to utilize low irradiance [49], they may be light-limited in the Antarctic turbid coastal waters or deeply mixed oceanic waters [50,51].

Table 2. Spearman's correlation between the studied variables. Statistically significant ($p < 0.05$) indicators are in bold. The description of the variables is in Table 1.

Variable	*T*	*S*	*PO4*	*Si*	*NO3*	*NO2*	*NH4*	*DO*	*FLUOR*
CPN	**0.59**	**−0.53**	−0.22	−0.22	**−0.45**	0.29	0.20	**0.78**	**0.37**
CP-ESD	−0.24	0.02	−0.14	0.28	0.29	−0.18	0.27	−0.15	−0.11
CPB	**0.54**	**−0.52**	−0.23	−0.16	**−0.40**	0.25	0.21	**0.74**	**0.36**
CP-CHL	−0.12	−0.06	**−0.32**	0.27	0.09	**−0.41**	**0.62**	0.04	−0.04
CP-PE	0.10	−0.06	−0.01	−0.13	0.03	0.00	0.28	0.11	−0.03
NPN	**0.74**	**−0.81**	0.32	0.24	**−0.59**	**0.56**	0.32	**0.60**	**0.73**
NP-ESD	−0.02	0.01	−0.32	−0.17	−0.10	−0.26	0.08	0.31	0.06
NPB	**0.68**	**−0.75**	0.12	0.10	**−0.63**	**0.42**	0.25	**0.73**	**0.73**
NP-CHL	0.01	−0.14	0.04	**0.44**	−0.16	−0.12	**0.34**	−0.15	0.12
TNPB	**0.59**	**−0.57**	−0.19	−0.14	**−0.45**	0.27	0.22	**0.77**	**0.42**
CPN%	**0.43**	**−0.33**	−0.31	**−0.32**	−0.30	0.15	0.07	**0.65**	0.15
CPB%	**0.47**	**−0.41**	−0.30	−0.25	−0.30	0.25	0.15	**0.65**	0.19
PPEN	**0.35**	**−0.39**	**0.41**	0.13	−0.30	0.24	0.17	0.21	**0.45**
PPE-ESD	**−0.85**	**0.78**	−0.28	−0.04	**0.62**	**−0.68**	−0.04	**−0.62**	**−0.47**
PPEB	0.06	−0.11	**0.34**	0.09	−0.09	−0.03	0.17	0.02	0.26

4.2. Cryptophyta

The distribution patterns of Chl-*a* and the total biomass of nanophytoplankton (*TNPB*) estimated by flow cytometry were similar, with the highest values at the same stations and depths (Figure 4). This provided evidence that nanophytoplankton was a major, if not dominant, component of the phytoplankton in the study site. To verify this suggestion, we estimated a potential contribution of CP to the total Chl-*a*, using different conversion factors: 0.2 pg Chl-*a* cell^{-1} [52] and 1.5 pg Chl-*a* cell^{-1} [53]. In the high Chl-*a* spot at station 6591 (1.28 μg Chl-*a* L^{-1}), the approximation of CP biomass in terms of Chl-*a* ranged from 0.31 to as high as 2.32 μg Chl-*a* L^{-1}, depending on which conversion factor is used. Additionally, we used the *TNPB*-to-*FLUOR* ratio as a measure of the nanophytoplankton contribution to the total phytoplankton biomass. The highest ratio values were observed in TBW with the maximum at station 6592 (Figure 4). Thus, the nanophytoplankton and CP could potentially dominate phytoplankton in TBW, where the phytoplankton bloom occurred.

The Cryptophyta biomass maximum (about 180 μg C L^{-1}) reported in our study is an outstanding characteristic for Antarctic waters. The importance of cryptophytes in different basins of the Southern Ocean has been reported earlier [1,2,54–57] but their maximum concentrations were much lower (between 0.3 and 6.0 × 10^6 cells L^{-1}) than our estimates. Garibotti et al. [3] have surprisingly revealed peak concentrations in the region of Anvers Island, reaching 369 μg C L^{-1}, i.e., close to our estimates. Therefore, our results widen the area of Cryptophyta blooms to the central Bransfield Strait and support the conclusion of the above authors that cryptophytes are a distinctive and annually recurrent component of Antarctic phytoplankton. Their blooms are increasingly becoming a peculiarity of the continental shelf west of the Antarctic Peninsula.

4.3. Linkage between Nanophytoplankton and Environmental Variables

All of the quantitative characteristics of the nanophytoplankton (*CPN*, *NPN*, *CPB*, *NPB*, *TNPB*) demonstrated a significant positive correlation with water temperature (*T*), dissolved oxygen (*DO*), and Chl-*a* fluorescence (*FLUOR*), while negative correlations were found with salinity (*S*) and nitrates (*NO3*) (Table 2). These environmental variables gradually changed with depth and in the transition from TBW to TWW, that explained well the above dependencies: in general, the nanophytoplankton abundances also decreased from the surface (TBW) to deeper layers (TWW) and from the northern (TBW) to the southern (TWW) stations along the transect. Thus, both CP and NP preferred warmer and fresher TBW, that supported earlier published observations [2,41,51,57–59]. The contribution of CP to the total nanophytoplankton abundance and biomass appeared the highest in TBW (Figure 5).

Chl-*a* fluorescence was significantly correlated with the total nanophytoplankton, especially with the NP concentrations (Table 2), most likely due to the higher NP abundance (*NPN*) and intracellular Chl-*a* content (*NP-CHL*) compared with the same characteristics in CP (Table 1). Intracellular Chl-*a* values in both CP and NP had a positive relationship with the ammonium concentration (*NH4*). Significant correlations have also been revealed between *NP-CHL* and *Si* (0.44), *CP-CHL* and *PO4* (−0.32), *CP-CHL* and *NO3* (−0.41) (Table 2).

It should be noted that a strong relationship between the nanophytoplankton abundance (*CPN*, *NPN*) and water temperature was found over the entire set of data (see the regression lines in Figure 6a,b). However, within each of the biotopes, TBW and TWW, the nature of the relationship was different. The *CPN* kept strong dependence (r^2 = 0.65) on temperature within TBW but the other links were lost (see the regressions represented with dashed lines in Figure 6a,b). Temperature did not appear to be a key factor controlling the NP abundance.

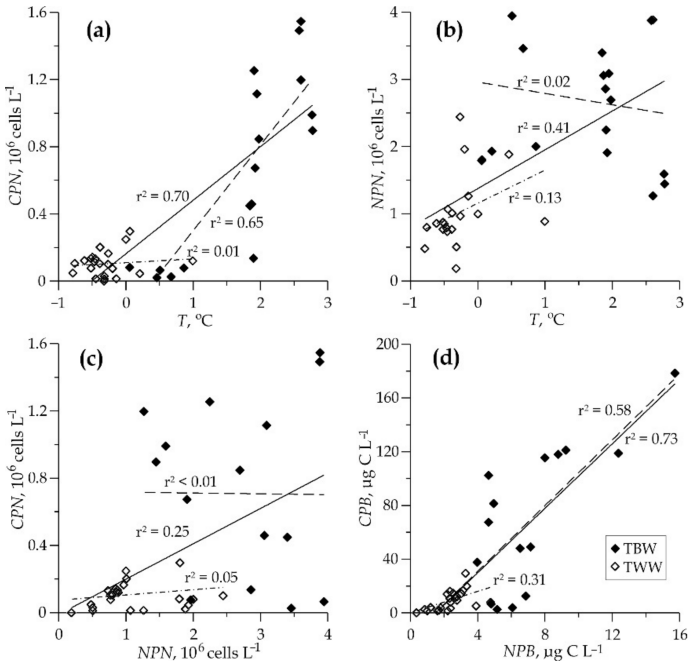

Figure 6. Relationships between: (**a**,**b**) the abundance of each group (*CPN*, *NPN*) and water temperature (*T*); (**c**) the cryptophyte (*CPN*) and other nanophytoplankton (*NPN*) abundances; (**d**) the cryptophyte (*CPB*) and other nanophytoplankton (*NPB*) biomasses. Samples from TBW (above 1 °C isotherm) and TWW (below 1 °C isotherm) water masses are represented with filled and empty symbols, respectively. Solid lines are regressions for the entire set of data, dashed ones are for individual biotopes. Description of the variables is in Table 1.

The CP and NP exhibited significant inter-correlation in terms of their biomass (r^2 = 0.73) but not of their abundance (r^2 = 0.25) (Figure 6c,d) that could provide evidence of their competition for the same resources. Yet again, the linkage between *CPB* and *NPB* were strong (r^2 = 0.58) in TBW, and poor (r^2 = 0.31) in TWW.

4.4. Comparing Nanophytoplankton from TBW and TWW

Cluster analysis allowed us to classify the nanophytoplankton samples, depending on the community structure (Figure 7a). A total of 4 sample groups were identified, 3 of which (the clusters 2 to 4) were within the TBW biotope (see the scheme of the cluster distribution in the water column in Figure 7b). The sample collected in the surface layer at station 6587 formed the cluster 4, owing to the outstanding microbial characteristics: the highest biomasses and average ESD of CP (178.5 µg C L^{-1}; 11.6 µm) and NP (15.7 µg C L^{-1}; 3.7 µm). The cluster 3 included 'patches' of nanophytoplankton at stations 6587 and 6591 within the TBW water mass (upper 50 m). In the cluster 2, *CPN* and *CPN%* significantly decreased. In the TWW biotope, the community was represented by the cluster 1 with low or undetectable microbial abundances (Figure 7b). Thus, the physical and chemical properties of the water masses deeply influenced the nanophytoplankton structure. The TBW biotope was characterized by much greater cell abundance and by a more diverse community with a pronounced dominance of Cryptophyta in terms of biomass.

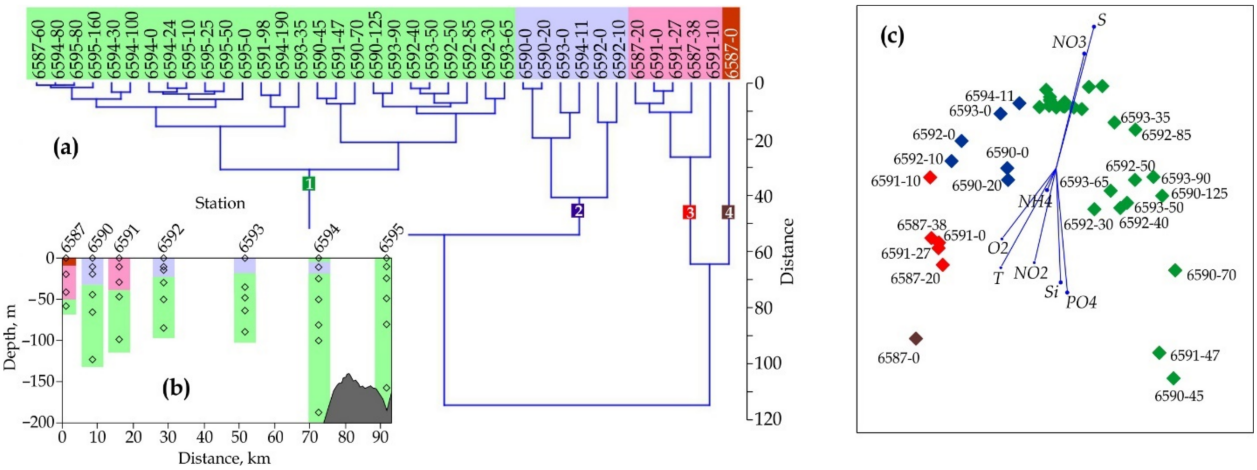

Figure 7. Cluster and non-metric multidimensional scaling (nMDS) analyses performed on the variables characterizing the nanophytoplankton community in the Bransfield Strait during austral summer, January 2020: (**a**) Dendrogram of a hierarchical cluster analysis with Euclidean distance measure, and four identified clusters; single samples are marked with a code indicating the station and depth of sampling; (**b**) Locations of nanophytoplankton assemblages identified by cluster analysis; background colors correspond to the cluster numbers in (**a**). (**c**) nMDS ordination of the nanophytoplankton samples with the environmental variables overlaid; symbol colors correspond to the cluster numbers in (**a**); single samples are marked with the code indicating the station number and the depth of sampling.

The ordination of the nanophytoplankton samples by nMDS produced similar results (Figure 7c) however, nMDS did not reveal a clear distinction between the sample clusters 1–4 revealed by the cluster analysis (shown in Figure 7c) in different colors). The clouds of dots corresponding to both the biotopes, TBW (the clusters 2–4) and TWW (the cluster 1), were distributed along the environmental vectors, which indicated a strong environmental control of nanophytoplankton. Distribution of the TBW-TWW fronts, anticyclonic eddies and their thermohaline structures, and nutrients are among the factors, which can control the community across the BS [60–62].

4.5. Cryptophyta Distribution Pattern in the Bransfield Strait

In general, the spatial distribution patterns of Chl-*a* fluorescence that we observed in the central BS were well aligned with the earlier long-term observations: the highest Chl-*a* was usually found close to the South Shetland Islands with the UML depth being negatively related to Chl-*a* [63]; at the well-stratified sites (TBW), with the euphotic layer varying from 40 to 50 m, the highest Chl-*a* was at the surface, while the weakly stratified sites (TWW) were associated with the low Chl-*a* and deeper euphotic layer [64].

However, the spatial patterns of cryptophytes in the coastal areas of the Antarctic Peninsula are more complicated. In the Eastern BS, Gonçalves-Araujo et al. [9] observed a dominance of microplanktonic diatoms and higher Chl-*a* within shallow upper mixed layers in TBW, close to the South Shetland Islands, while TWW was primarily characterized by lower Chl-*a* within well-mixed water column and dominated by nanoplanktonic flagellates (including haptophytes and cryptophytes). This contradicted our observations of coincident maxima of the Chl-*a* fluorescence and the cryptophyte concentration within the TBW surface layer with lower salinity and higher temperature (>1 °C).

According to Schofield et al. [65], peak populations of cryptophytes were observed in the coastal areas of the West Antarctic Peninsula with lower salinity (33.75 to 32.5 psu) and colder water (−1 to 1 °C), while they were absent at higher temperatures (>1 °C) and salinities (>33.75 psu). On the contrary, Mendes et al. [18] provided different data on the distribution of cryptophyte biomass in the Gerlache Strait, which was mostly dependent on the sea surface temperature, rather than salinity. The authors found that cryptophytes were strongly associated with high temperature, water column stability, and Chl-*a*, and negatively associated with nutrient concentrations, UMLD, and salinity, which was in good agreement with our observations and a few earlier reports [2,51,57,59,64].

An explanation of the phenomenon may consist in early retreat of sea ice, which, together with the increase in sea surface temperature, leads to the development of a shallow mixing layer and strong vertical water column stratification. The latter confines phytoplankton near the surface under high irradiance [66]. Mendes et al. [18] hypothesized that the dominance of cryptophytes in the coastal waters of the Antarctic Peninsula is just associated with their ability to grow under high irradiance exposure due to their pigment protection capability.

Thus, the increase in melt-water input may potentially enlarge the spatial and temporal extent of cryptophytes [8]. Our study supports this suggestion, providing evidence of extremely high cryptophyte biomass within low-salinity, high-temperature TBW. Historical data also show an emerging dominance of cryptophytes and other phytoflagellates in low-saline coastal waters [43,56,57,67–70]. As a consequence of these processes, zooplankton community structure undergoes cascade changes [16,71] leading to an increase in salp abundance and concurrent variations in penguin migration patterns [72]. If this trend persists for a long time, the food web shifts will eventually impact biogeochemical cycling in the Antarctic coastal waters.

5. Conclusions

In this study, we found higher abundances and biomasses of nanophytoplankton in the warmer and fresher transitional water mass with Bellingshausen Sea influence (TBW). This biotope was characterized by a more diverse community with a pronounced dominance of cryptophytes in terms of biomass (up to 180 μg C L^{-1}). Patches of the highest cryptophyte abundance were observed in the euphotic layer around the jet of the Bransfield Current. In the transitional water mass with Weddell Sea influence (TWW), they were scarce or undetectable, especially in the deeper layers. Our results widen the area of Cryptophyta blooms to the central Bransfield Strait and support the conclusion that these small eukaryotes are a distinctive and annually recurrent component of Antarctic phytoplankton.

In the study site, picophytoplankton were represented by picoeukaryotes and characterized by low abundances (about 0.87×10^6 cells L^{-1}) and patchy distribution. They

preferred deeper, colder layer, thus, demonstrating their association with TWW and the frontal zone between the water masses.

Our results support the hypothesis that increasing melt-water input can potentially increase spatial and temporal extent of cryptophytes in the Antarctic region.

Author Contributions: Conceptualization, V.M.; methodology, V.M., E.S., A.P., V.A. and E.M.; formal analysis, V.M. and A.-Y.T.; data curation, V.M., A.P. and E.M.; writing—original draft preparation, V.M.; writing—review and editing, V.M. and A.-Y.T. All authors have read and agreed to the published version of the manuscript.

Funding: This research was conducted in the frame of the Russian state assignments No. AAAA-A19-119100290162-0 (V.M. and E.S.) and 0128-2021-0017 (E.M., A.P. and V.A.), and supported by RFBR, grant number 21-55-52001 (V.M. and E.S.), and the Ministry of Science and Technology, ROC (Taiwan), grant number NSC 109-2611-M-019-013 (A.-Y.T.).

Conflicts of Interest: The authors declare no conflict of interest.

References

1. Rodriguez, F.; Varela, M.; Zapata, M. Phytoplankton assemblages in the Gerlache and Bransfield Straits (Antarctic Peninsula) determined by light microscopy and CHEMTAX analysis of HPLC pigment data. *Deep Sea Res. Part II Top. Stud. Oceanogr.* **2002**, *49*, 723–747. [CrossRef]
2. Garibotti, I.A.; Vernet, M.; Ferrario, M.E.; Smith, R.C.; Ross, R.M.; Quetin, L.B. Phytoplankton spatial distribution patterns along the western Antarctic Peninsula (Southern Ocean). *Mar. Ecol. Prog. Ser.* **2003**, *261*, 21–39. [CrossRef]
3. Garibotti, I.A.; Vernet, M.; Ferrario, M.E. Annually recurrent phytoplanktonic assemblages during summer in the seasonal ice zone west of the Antarctic Peninsula (Southern Ocean). *Deep Sea Res. Part I Oceanogr. Res. Pap.* **2005**, *52*, 1823–1841. [CrossRef]
4. Kozlowski, W.A.; Deutschman, D.; Garibotti, I.; Trees, C.; Vernet, M. An evaluation of the application of CHEMTAX to Antarctic coastal pigment data. *Deep Sea Res. Part I Oceanogr. Res. Pap.* **2011**, *58*, 350–364. [CrossRef]
5. Mendes, C.R.B.; de Souza, M.S.; Garcia, V.M.T.; Leal, M.C.; Brotas, V.; Garcia, C.A.E. Dynamics of phytoplankton communities during late summer around the tip of the Antarctic Peninsula. *Deep Sea Res. Part I Oceanogr. Res. Pap.* **2012**, *65*, 1–14. [CrossRef]
6. Prézelin, B.B.; Hofmann, E.E.; Mengelt, C.; Klinck, J.M. The linkage between Upper Circumpolar Deep Water (UCDW) and phytoplankton assemblages on the west Antarctic Peninsula continental shelf. *J. Mar. Res.* **2000**, *58*, 165–202. [CrossRef]
7. Moline, M.A.; Prezelin, B.B. Long-term monitoring and analyses of physical factors regulating variability in coastal Antarctic phytoplankton biomass, *in situ* productivity and taxonomic composition over subseasonal, seasonal and interannual time scales. *Mar. Ecol. Prog. Ser.* **1996**, *145*, 143–160. [CrossRef]
8. Moline, M.A.; Claustre, H.; Frazer, T.K.; Schofield, O.; Vernet, M. Alteration of the food web along the Antarctic Peninsula in response to a regional warming trend. *Glob. Chang. Biol.* **2004**, *10*, 1973–1980. [CrossRef]
9. Gonçalves-Araujo, R.; de Souza, M.S.; Tavano, V.M.; Garcia, C.A.E. Influence of oceanographic features on spatial and interannual variability of phytoplankton in the Bransfield Strait, Antarctica. *J. Mar. Syst.* **2015**, *142*, 1–15. [CrossRef]
10. Mendes, C.R.B.; Tavano, V.M.; Leal, M.C.; de Souza, M.S.; Brotas, V.; Garcia, C.A.E. Shifts in the dominance between diatoms and cryptophytes during three late summers in the Bransfield Strait (Antarctic Peninsula). *Polar Biol.* **2013**, *36*, 537–547. [CrossRef]
11. Haberman, K.L.; Ross, R.M.; Quetin, L.B. Diet of the Antarctic krill (*Euphausia superba* Dana): II Selective grazing in mixed phytoplankton assemblages. *J. Exper. Mar. Biol. Ecol.* **2003**, *283*, 97–113. [CrossRef]
12. Moline, M.A.; Claustre, H.; Frazer, T.K.; Grzymski, J.; Vernet, M. Changes in phytoplankton assemblages along the Antarctic Peninsula and potential implications for the Antarctic food web. In *Antarctic Ecosystems: Models for Wider Ecological Understanding*; Davidson, W., Howard-Williams, C., Broady, P., Eds.; University of Canterbury: Christchurch, New Zealand, 2001.
13. McClatchie, S.; Boyd, C.M. Morphological study of sieve efficiencies and mandibular surfaces in the Antarctic krill, Euphausia superba. *Can. J. Fish. Aquat. Sci.* **1983**, *40*, 955–967. [CrossRef]
14. Boyd, C.M.; Heyraud, M.; Boyd, C.N. Feeding of the Antarctic krill Euphausia superba. *J. Crustacean Biol.* **1984**, *4*, 123–141. [CrossRef]
15. Montes-Hugo, M.; Doney, S.C.; Ducklow, H.W.; Fraser, W.; Martinson, D.; Stammerjohn, S.E.; Schofield, O. Recent changes in phytoplankton communities associated with rapid regional climate change along the western Antarctic Peninsula. *Science* **2009**, *323*, 1470–1473. [CrossRef] [PubMed]
16. Loeb, V.; Siegel, V.; Holm-Hansen, O.; Hewitt, R.; Fraser, W.; Trivelpiece, W.; Trivelpiece, S. Effects of sea-ice extent and krill or salp dominance on the Antarctic food web. *Nature* **1997**, *387*, 897–900. [CrossRef]
17. Castro, C.G.; Ríos, A.F.; Doval, M.D.; Pérez, F.F. Nutrient utilisation and chlorophyll distribution in the Atlantic sector of the Southern Ocean during Austral summer 1995–96. *Deep Sea Res.* **2002**, *49*, 623–641. [CrossRef]
18. Mendes, C.R.B.; Tavano, V.M.; Dotto, T.S.; Kerr, R.; De Souza, M.S.; Garcia, C.A.E.; Secchi, E.R. New insights on the dominance of cryptophytes in Antarctic coastal waters: A case study in Gerlache Strait. *Deep Sea Res. Part II Top. Stud. Oceanogr.* **2018**, *149*, 161–170. [CrossRef]

19. Polukhin, A.A.; Morozov, E.G.; Tishchenko, P.P.; Frey, D.I.; Artemiev, V.A.; Borisenko, G.V.; Vidnichuk, A.V.; Marina, E.N.; Medvedev, E.V.; Popov, O.S.; et al. Water structure in the Bransfield Strait (Antarctica) in January 2020: Hydrophysical, optical and hydrochemical features. *Oceanology* **2021**, *61*, 632–644. [CrossRef]
20. Tokarczyk, R. Classification of water masses in the Bransfield Strait and southern part of the Drake Passage using a method of statistical multidimensional analysis. *Pol. Res.* **1987**, *8*, 333–366.
21. Garcıa, M.; Castro, C.; Rıos, A. Water masses and distribution of physico-chemical properties in the Western Bransfield Strait and Gerlache Strait during Austral summer 1995/96. *Deep Sea Res. Part II Top. Stud. Oceanogr.* **2002**, *49*, 585–602. [CrossRef]
22. Bordovsky, O.K.; Chernyakova, A.M. *Modern Methods of Hydrochemical Studies of the Ocean*; IO RAS: Moscow, Russia, 1992; pp. 1–200. (In Russian)
23. Solorzano, L. Determination of ammonia in natural waters by phenol-hypochlorite method. *Limnol. Oceanogr.* **1969**, *14*, 799–801.
24. Strickland, J.D.H.; Parsons, T.R. *A Practical Handbook of Seawater Analysis*, 2nd ed.; Bulletin of Fisheries Research Board of Canada: Ottawa, ON, Canada, 1972; pp. 1–328.
25. Grasshoff, K.; Kremling, K.; Ehrhardt, M. *Methods of Seawater Analysis*; John Wiley & Sons: New York, NY, USA, 2009; pp. 1–599.
26. Parsons, T.R. *A Manual of Chemical & Biological Methods for Seawater Analysis*; Elsevier: Amsterdam, The Netherlands, 2013; pp. 1–188.
27. Hoef-Emden, K.; Marin, B.; Melkonian, M. Nuclear and nucleomorph SSU rDNA phylogeny in the Cryptophyta and the evolution of cryptophyte diversity. *J. Mol. Evol.* **2002**, *55*, 161–179. [CrossRef] [PubMed]
28. Six, C.; Thomas, J.C.; Brahamsha, B.; Lemoine, Y.; Partensky, F. Photophysiology of the marine cyanobacteria *Synechococcus* sp. WH8102, a new model organism. *Aquat. Microb. Ecol.* **2004**, *35*, 17–29. [CrossRef]
29. Marie, D.; Simon, N.; Vaulot, D. Phytoplankton cell counting by flow cytometry. In *Algal Culturing Techniques*; Andersen, R.A., Ed.; Elsevier: Amsterdam, The Netherlands, 2005; pp. 253–267.
30. Olson, R.J.; Zettler, E.R.; DuRand, M.D. Phytoplankton analysis using flow cytometry. In *Handbook of Methods in Aquatic Microbial Ecology*; CRC Press: Boca Raton, FL, USA, 1993; pp. 175–186.
31. Alvarez, E.; Nogueira, E.; López-Urrutia, Á. In vivo single-cell fluorescence and size scaling of phytoplankton chlorophyll content. *Appl. Environ. Microbiol.* **2017**, *83*, 1–16. [CrossRef] [PubMed]
32. Worden, A.; Nolan, J.; Palenik, B. Assessing the dynamics and ecology of marine picophytoplankton: The importance of the eukaryotic component. *Limnol. Oceanogr.* **2004**, *49*, 168–179. [CrossRef]
33. Garrison, D.; Gowing, M.; Hughes, M. Microbial food web structure in the Arabian Sea: A US JGOFS study. *Deep Sea Res. Part II* **2000**, *47*, 1387–1422. [CrossRef]
34. Hammer, O.; Harper, D.A.T.; Ryan, P.D. PAST: Paleontological statistics software package for education and data analysis. *Paleontol. Electron.* **2001**, *4*, 1–9.
35. Zhou, M.; Niiler, P.P.; Zhu, Y.; Dorland, R.D. The western boundary current in the Bransfield Strait, Antarctica. *Deep Sea Res. I* **2006**, *53*, 1244–1252. [CrossRef]
36. Niiler, P.P.; Amos, A.; Hu, J.-H. Water masses and 200 m relative geostrophic circulation in the western Bransfield Strait region. *Deep Sea Res.* **1991**, *38*, 943–959. [CrossRef]
37. Garcia, M.A.; López, O.; Sospedra, J.; Espino, M.; Gracia, V.; Morrison., G.; Arcilla, A.S. Mesoscale variability in the Bransfield Strait region (Antarctica) during Austral summer. *Ann. Geophys.* **1994**, *12*, 856–867. [CrossRef]
38. Sangrà, P.; Gordo, C.; Hernández-Arencibia, M.; Marrero-Díaz, A.; Rodríguez-Santana, A.; Stegner, A.; Pichon, T. The Bransfield current system. *Deep Sea Res. I* **2011**, *58*, 390–402. [CrossRef]
39. Jiang, M.; Charette, M.A.; Measures, C.I.; Zhu, Y.; Zhou, M. Seasonal cycle of circulation in the Antarctic Peninsula and the off-shelf transport of shelf waters into southern Drake Passage and Scotia Sea. *Deep Sea Res. Part II Top. Stud. Oceanogr.* **2013**, *90*, 15–30. [CrossRef]
40. Morozov, E.G. Currents in Bransfield Strait. *Dokl. Earth Sci.* **2007**, *415*, 984–986. [CrossRef]
41. Holm-Hansen, O.; Mitchell, B.G. Spatial and temporal distribution of phytoplankton and primary production in the western Bransfield Strait region. *Deep Sea Res. II* **1991**, *39*, 961–980. [CrossRef]
42. Dierssen, H.M.; Smith, R.C. Case 2 Antarctic coastal waters: The bio-optical properties of surface meltwater. In Proceedings of the Ocean Optics XV, Kailua-Kona, HI, USA, 16–20 October 2000.
43. McMinn, A.; Hodgson, D. Summer phytoplankton succession in Ellis Fjord, eastern Antarctica. *J. Plankton Res.* **1993**, *15*, 925–938. [CrossRef]
44. Bouman, H.A.; Ulloa, O.; Barlow, R.; Li, W.K.; Platt, T.; Zwirglmaier, K.; Sathyendranath, S. Water-column stratification governs the community structure of subtropical marine picophytoplankton. *Environ. Microbiol. Rep.* **2011**, *3*, 473–482. [CrossRef]
45. Buitenhuis, E.T.; Li, W.K.; Vaulot, D.; Lomas, M.W.; Landry, M.R.; Partensky, F.; McManus, G.B. Picophytoplankton biomass distribution in the global ocean. *Earth Syst. Sci. Data* **2012**, *4*, 37–46. [CrossRef]
46. Agawin, N.S.; Agustí, S.; Duarte, C.M. Abundance of Antarctic picophytoplankton and their response to light and nutrient manipulation. *Aquat. Microb. Ecol.* **2002**, *29*, 161–172. [CrossRef]
47. Weber, L.H.; El-Sayed, S.Z. Contribution of the net-, nano and picoplankton standing crop and primary productivity in the Southern Ocean. *J. Plankton Res.* **1987**, *9*, 973–994. [CrossRef]
48. Lin, L.; He, J.; Zhao, Y.; Zhang, F.; Cai, M. Flow cytometry investigation of picoplankton across latitudes and along the circum Antarctic Ocean. *Acta Oceanol. Sin.* **2012**, *31*, 134–142. [CrossRef]

49. Morris, I.; Glover, H. Physiology of photosynthesis by marine coccoid cyanobacteria—Some ecological implications. *Limnol. Oceanogr.* **1981**, *26*, 957–961. [CrossRef]
50. Sakshaug, E.; Holm-Hansen, O. Photoadaptation in Antarctic phytopfankton: Variations in growth rate, chemical composition and P versus I curves. *J. Plankton Res.* **1986**, *8*, 459–473. [CrossRef]
51. Mitchell, B.G.; Holm-Hansen, O. Observations of modeling of the Antarctic phytoplankton crop in relation to mixing depth. *Deep Sea Res. Part A Oceanogr. Res. Pap.* **1991**, *38*, 981–1007. [CrossRef]
52. Vaillancourt, R.D.; Brown, C.W.; Guillard, R.R.L.; Balch, W.M. Light scattering properties of marine phytoplankton: Relationships to cell size, chemical composition and taxonomy. *J. Plankton Res.* **2004**, *26*, 191–212. [CrossRef]
53. Eriksen, N.T.; Poulsen, B.R.; Iversen, J.L. Dual sparging laboratory-scale photobioreactor for continuous production of microalgae. *J. Appl. Phycol.* **1998**, *10*, 377–382. [CrossRef]
54. Jacques, G.; Panouse, M. Biomass and composition of size fractionated phytoplankton in the Weddell-Scotia Confluence area. *Polar Biol.* **1991**, *5*, 315–328. [CrossRef]
55. Kopczynska, E.E. Distribution of microflagellates and diatoms in the sea-ice zone between Elephant Island and the South Orkney Islands (December 1988–January 1989). *Pol. Polar Res.* **1991**, *12*, 515–528.
56. Buma, A.G.J.; Gieskes, W.W.C.; Thomsen, H.A. Abundance of Cryptophyceae and chlorophyll b-containing organisms in the Weddell-Scotia Confluence area in the spring of 1988. In *Weddell Sea Ecology*; Hempel, G., Ed.; Springer: Berlin/Heidelberg, Germany, 1992; pp. 43–52.
57. Kang, S.-H.; Lee, S. Antarctic phytoplankton assemblage in the western Bransfield Strait region, February 1993: Composition, biomass, and mesoscale distributions. *Mar. Ecol. Prog. Ser.* **1995**, *129*, 253–267. [CrossRef]
58. Holm-Hansen, O.; Mitchell, B.G.; Hewes, C.D.; Karl, D.M. Phytoplankton blooms in the vicinity of Palmer Station, Antarctica. *Polar Biol.* **1989**, *10*, 49–57. [CrossRef]
59. Smith, W.O., Jr.; Sakshaug, E. Polar Phytoplankton. In *Polar Oceanography, Part B*; Smith, W.O., Jr., Ed.; Academic Press: London, UK, 1990; pp. 477–525.
60. García-Muñoz, C.; Lubián, L.M.; García, C.M.; Marrero-Díaz, Á.; Sangrà, P.; Vernet, M. A mesoscale study of phytoplankton assemblages around the South Shetland Islands (Antarctica). *Polar Biol.* **2013**, *36*, 1107–1123. [CrossRef]
61. Mura, M.P.; Satta, M.P.; Agustí, S. Water-mass influences on summer Antarctic phytoplankton biomass and community structure. *Polar Biol.* **1995**, *15*, 15–20. [CrossRef]
62. Sangrà, P.; García-Muñoz, C.; García, C.M.; Marrero-Díaz, Á.; Sobrino, C.; Mouriño-Carballido, B.; Hernández-Arencibia, M. Coupling between upper ocean layer variability and size-fractionated phytoplankton in a non-nutrient-limited environment. *Mar. Ecol. Prog. Ser.* **2014**, *499*, 35–46. [CrossRef]
63. Hewes, C.D.; Reiss, C.S.; Holm-Hansen, O. A quantitative analysis of sources for summertime phytoplankton variability over 18 years in the South Shetland Islands (Antarctica) region. *Deep Sea Res. Part I Oceanogr. Res. Pap.* **2009**, *56*, 1230–1241. [CrossRef]
64. Holm-Hansen, O.; Hewes, C.D.; Villafane, V.E.; Helbling, E.W.; Silva, N.; Amos, T. Distribution of phytoplankton and nutrients in relation to different water masses in the area around Elephant Island, Antarctica. *Polar Biol.* **1997**, *18*, 145–153. [CrossRef]
65. Schofield, O.; Saba, G.; Coleman, K.; Carvalho, F.; Couto, N.; Ducklow, H.; Montes-Hugo, M. Decadal variability in coastal phytoplankton community composition in a changing West Antarctic Peninsula. *Deep Sea Res. Part I Oceanogr. Res. Pap.* **2017**, *124*, 42–54. [CrossRef]
66. Moreau, S.; Ferreyra, G.A.; Mercier, B.; Lemarchand, K.; Lionard, M.; Roy, S.; Mostajir, B.; Van Hardenberg, B.; Demers, S. Variability of the microbial community in the western Antarctic Peninsula from late fall to spring during a low ice cover year. *Polar Biol.* **2010**, *33*, 1599–1614. [CrossRef]
67. Ferreyra, G.A.; Tomo, A.P. Variacion estational de las diatomeas planctonicas en Puerto Paraiso-I. *Contrib. Del Inst. Antart. Argentio* **1979**, *264*, 149–184.
68. Whitaker, T.M. Primary production of phytoplankton off Signy Island, South Orkneys, the Antarctic. *Proc. R. Soc. Lond. Ser. B Biol. Sci.* **1982**, *214*, 169–189.
69. Krebs, W.N. Ecology of neritic marine diatoms, Arthur Harbor, Antarctica. *Micropaleontology* **1983**, *29*, 267–297. [CrossRef]
70. Kopczynska, E.E. Dominance of microflagellates over diatoms in the Antarctic areas of deep vertical mixing and krill concentrations. *J. Plankton Res.* **1992**, *14*, 1031–1054. [CrossRef]
71. Walsh, J.J.; Dieterle, D.A.; Lenes, J. A numerical analysis of carbon dynamics of the Southern Ocean phytoplankton community: The roles of light and grazing in effecting both sequestration of atmospheric CO_2 and food availability to larval krill. *Deep Sea Res.* **2001**, *48*, 1–48. [CrossRef]
72. Ainley, D.G.; Ballard, G.; Emslie, S.D. Adélie penguins and environmental change. *Science* **2003**, *300*, 429–430. [CrossRef] [PubMed]